3 Scale Effects in Creep Parameters

A series of in-situ creep were conducted on claystone specimens in order to investigate the influence of scale effects on creep parameters. The experimental setup for these tests is similar to the one shown in Figure 1, with variable specimen sizes from $10 \times 10 \times 10cm^3$ to $100 \times 100 \times 100cm^3$. The experimental results are shown in Figure 4, where creep parameters are normalized against the number of rock blocks or the overall size of the specimens. The following relations are obtained from the experimental results:

(1) **Scale Effects on Initial Creep Stresses.** As shown in Figures 4(a) and (e), the scale effect on initial creep stresses is defined as

$$\begin{cases} \frac{\sigma_i}{\sigma_{imax}} = 1.8023N^{-0.4960} \\ \frac{\sigma_i}{\sigma_{imax}} = 3.8106L^{-0.5699} \end{cases} \tag{1}$$

where σ_i and σ_{imax} are, respectively, the initial creep stress for the fractured rock mass and the initial creep stress for the intact rock; N and L are, respectively, the number of rock blocks contained in a rock specimen and the overall size of that specimen.

(2) **Scale Effects on Failure Creep Stresses.** As shown in Figures 4(b) and (f), the scale effect on failure creep stresses is defined as

$$\begin{cases} \frac{\sigma_c}{\sigma_{cmax}} = 2.3852N^{-0.6002} \\ \frac{\sigma_c}{\sigma_{cmax}} = 4.4575L^{-0.6354} \end{cases} \tag{2}$$

where σ_c and σ_{cmax} are, respectively, the failure creep stress for the fractured rock mass and the failure creep stress for the intact rock.

(3) **Scale Effects on Deformation Moduli.** As shown in Figures 4(c) and (g), the scale effect on deformation moduli is defined as

$$\begin{cases} \frac{E}{E_{max}} = 9.0806N^{-1.1588} \\ \frac{E}{E_{max}} = 50.0740L^{-1.3544} \end{cases} \tag{3}$$

where E and E_{max} are, respectively, the deformation modulus for the fractured rock mass and the deformation modulus for the intact rock.

(4) **Scale Effects on Viscosity Coefficients.** As shown in Figures 4(d) and (h), the scale effect on viscosity coefficients is defined as

$$\begin{cases} \frac{\eta}{\eta_{max}} = 13.9320N^{-1.6150} \\ \frac{\eta}{\eta_{max}} = 25.0730L^{-1.3555} \end{cases} \tag{4}$$

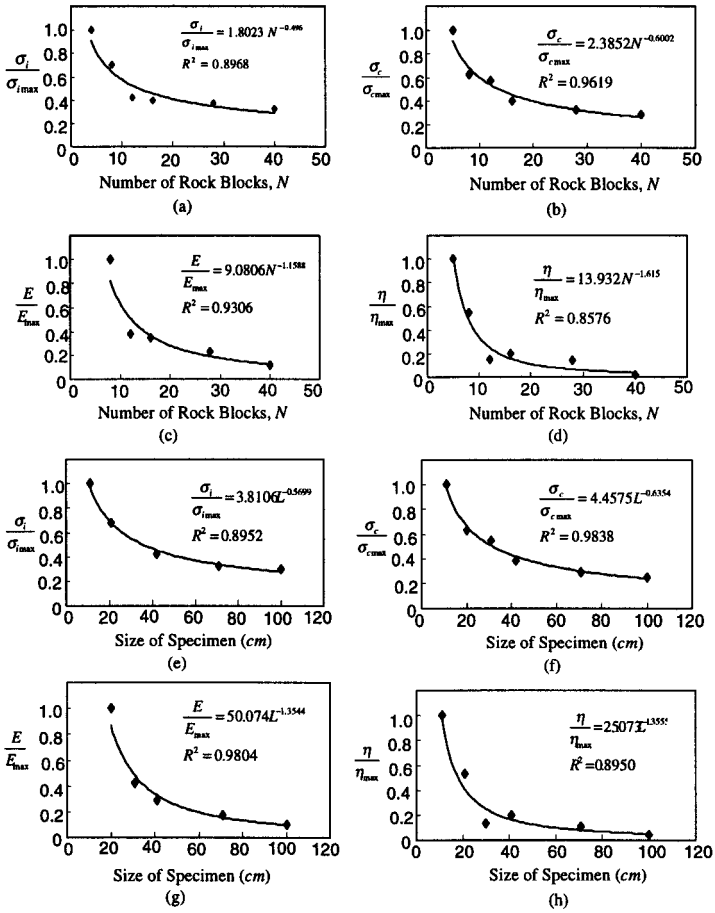

Figure 4: Scale effects in the creep parameters of fractured rock masses. The effect of the number of rock blocks on the initial creep stress, failure stress, elastic modulus and viscosity are shown in figures (a) through (d). Effects of the specimen sizes on the initial creep stress, failure stress, elastic modulus and viscosity are shown in figures (e) through (h).

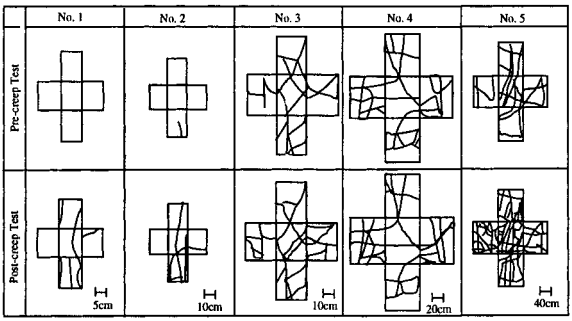

Figure 5: Comparison of failure modes between pre- and post-creep tests under different scales.

where η and η_{max} are, respectively, the viscosity coefficient for the fractured rock mass and the viscosity coefficient for the intact rock.

Relations, 1 through 4, may be defined, in a unified form, as

$$\frac{CP}{CP_{max}} = AS^{-B} \tag{5}$$

where CP and CP_{max} are creep parameters (σ_i, σ_c, E, and η, or σ_{imax}, σ_{cmax}, E_{max}, and η_{max}); A and B are constants, and S is the number of rock blocks contained in a rock specimen or the overall size of that specimen.

4 Scale Effects in Creep Failures

A series of creep tests were conducted to investigate scale effects on creep failure modes of rock masses. The sizes of five creep test specimens, as shown in Figure 5, are $10 \times 10 \times 10cm^3$ (No.1), $20 \times 20 \times 20cm^3$ (No.2), $30 \times 30 \times 30cm^3$ (No.3), $70 \times 70 \times 70cm^3$ (No.4), and $100 \times 100 \times 100cm^3$ (No.5). The number of fractures in the specimens increase with increasing specimen size. Among them, specimen No.1 contains no fractures, and the resulting failure mode is tensile fracturing; specimen, No.2, contains only one fracture, and the resulting failure mode is tensile fracturing through this pre-existing fracture; specimens, No.3 and No.4, contain a number of well-connected fractures, and the failure modes are flow-sliding through the pre-existing fractures; specimen, No.5, has the essential characteristics of the sampled rock mass, with fractures ($NE80^0/NW50^0$,

$NW40^0/NW40^0$, and $NE10^0/NW25^0$) forming a plane of slippage. The sliding is towards $NE25^0$, with a plunge of 24^0 below the horizontal, resulting in a failure mode representing differential flow-failure.

The experimental results, as shown in Figure 5, indicate that rock masses, sampled at different scales, may fail under different mechanisms and modes. This results from the different number of fractures present within the sampled volume, their mixed strength and geometric characteristics, and the additional degrees of freedom that this affords the failure process.

5 Conclusions

Three types of scale effects have been studied in this work to define the influence of creep deformation on the failure of fractured rock masses. These are:

(1) Scale effects on creep failure mechanisms;

(2) Scale effects on creep parameters;

(3) Scale effects on creep failure modes.

Caution should be applied when using the upscaling rules, developed in this study, in other situations. In particular, attention should be paid to the type of rock, and to the experimental conditions.

Acknowledgments

The work reported in this paper has been supported by the State Government of Western Australia through the Department of Commerce and Trade, Centres of Excellence Program. The fund is provided through the Australian Center for Geomechanics. The completion of the creep experiments has been supported by the Chinese National Foundation of Science (49472165) and the Chinese Academy of Sciences (KZ952-J1-003). This support is gratefully acknowledged. The helpful comments of two anonymous reviewers are also gratefully acknowledged.

References

Al-Harthi, A. A. and Hencher, S. R. (1993). On the effect of block size on the shear behavior of jointed rock masses. In Cunha, A. P. D., editor, *Scale Effects in Rock Masses*, pages 205–210.

Berry, D. S. (1963). Ground movement considered as an elastic phenomenon. *The Mining Engineer*, 37:28–39.

Cuisiat, F. D. and Haimson, B. C. (1993). The scale dependency of in-situ rock stress measurements. In Cunha, A. P. D., editor, *Scale Effects in Rock Masses*, pages 15–26.

Cunha, A. P. d. (1993). Scale effects in rock engineering - a general report on papers to the lisbon workshop. In Cunha, A. P. D., editor, *Scale Effects in Rock Masses*, pages 27–38.

Exadaktylos, G. E. and Tsoutrelis, C. E. (1993). Scale effect on rock mass strength and stability. In Cunha, A. P. D., editor, *Scale Effects in Rock Masses*, pages 101–110.

Gelhar, L. W. and Welty, C. (1992). A critical review of data on field-scale dispersion in aquifer. *Water Resources Research*, 22(7):1955–1974.

Hackett, P. (1959). An elastic analysis of rock movement caused by mining. *Transactions, Institute of Mining Engineering*, 118(Part 7):421–433.

Hackett, P. (1964). Prediction of rock movement by elastic theory compared with in-situ measurement. *Rock Mechanics and Engineering Geology*, Supplement 1:88–162.

Mohammad, N., Reddish, D. J., and Stace, L. R. (1997). The relation between in-situ and laboratory rock properties used in numerical modeling. *Int. J. Rock Mech. & Min. Sci.*, 34(2):289–297.

Moon, H. K. and Kim, C. Y. (1993). Scale effects in the elastic moduli and strength of jointed rock masses. In Cunha, A. P. D., editor, *Scale Effects in Rock Masses*, pages 39–48.

Ohnishi, Y., Herda, H., and Yoshinaka, R. (1993). Shear strength scale effect and the geometry of single and repeated rock joints. In Cunha, A. P. D., editor, *Scale Effects in Rock Masses*, pages 167–174.

Voight, B. (1970). State of predictive art in subsidence engineering. *J. Soil Mech. & Foundations Division, Proc. Of the American Society of Civil Engineers.*

Yoshinaka, R., Yoshida, J., Arai, H., and Arisaka, S. (1993). Scale effects on shear strength and deformability of rock joints. In Cunha, A. P. D., editor, *Scale Effects in Rock Masses*, pages 143–150.

Crack Kinematics of Rock-Like Materials by Quantitative Acoustic Emission

Masayasu Ohtsu

Abstract

The moment tensor corresponding to acoustic emission (AE) source contains kinematical information on crack motion in a material. In order to determine the moment tensor components from AE waveforms, the SiGMA (simplified Green's functions for moment tensor analysis) procedure is developed, where AE sources can be located, classified into tensile cracks and shear cracks, and then the directions of crack motions are determined.

In the present paper, the SiGMA procedure is further extended in rock-like materials, and a crack micrograpy is proposed. To this end, a relation between a damage parameter in damage mechanics and the moment tensor is clarified. Thus, damage evolution of the notched beam under bending is estimated from the trace components of the moment tensor. The scalar damage parameter is closely related with the crack density consisting of the crack volume. Therefore, the crack volumes are quantitatively estimated in uniaxial compression tests of plate specimens with a slit. In the linear elastic fracture mechanics (LEFM), the direction of crack extension can be determined from the concept of the maximum circumferential stress. Since the direction of crack motion can be derived from the eigenvectors of the moment tensor, the relation is applied to estimate the normalized stress intensity factors.

Introduction

Acoustic emission (AE) is defined as the generation of elastic waves due to cracking in materials. Therefore, AE techniques are extensively applied to detect cracks for inspection and to do research on failure mechanisms. Theoretical research of AE has been conducted on the basis of the elastodynamics and the dislocation theory. Thus, a generalized theory is presented by Ohtsu and Ono (1984). AE waves are, in principle, generated by crack motions, which correspond to AE sources. In this case, crack dynamics normally consists of crack kinetics and crack kinematics. The former is represented by the source time function which can be determined from the deconvolution analysis. The latter is associated with the moment tensor. In order to determine the moment tensor components from AE waveforms, a simplified and stable procedure is developed as a SiGMA procedure by Ohtsu (1991).

Professor, Department Civil Engineering and Architecture, Kumamoto University, 2-39-1 Kurokami, Kumamoto 860-8555, Japan

Crack kinematics obtained from the moment tensor readily lead to micrographical approach of nucleated cracks. Thus, the SiGMA procedure is further extended in rock-like materials, and a crack micrograpy is proposed here. The classification of crack type and the determination of crack orientation are discussed on the basis of the eigenvalue analysis of the moment tensor. From the continuous damage mechanics by Kachanov (1992), a relation between a damage parameter and the moment tensor components is studied. Then, the crack volume is quantitatively estimated in combination with AE sensor calibration. The maximum circumferential stress concept in the linear elastic fracture mechanics (LEFM) dictates a relation between the direction of crack extension and the stress intensity factors. Consequently, the crack orientation analyzed by the SiGMA is attempted to be applied to estimate the normalized stress intensity factors.

Procedure for Micrography

(1) SiGMA

Crack motion vector $\mathbf{b}(\mathbf{y},t)$ at AE source can be defined on crack surface F along with crack normal vector $\mathbf{n}$. As shown in Fig. 1, this crack motion is equivalently represented by moment tensor, $\mathbf{m}$. Mathematically, crack motion vector at point $\mathbf{y}$ is set to be equal to $b(\mathbf{y})\mathbf{l}S(t)$, where $b(\mathbf{y})$ represents the magnitude of crack displacement, $\mathbf{l}$ is the direction vector of crack motion $\mathbf{b}$, and $S(t)$ is the source-time function. Then, the following integration over the crack surface F leads to moment tensor, m_{pq},

$$\int_F C_{pqkl}\,[b(\mathbf{y})l_k S(t)]\,n_l\,dS = [C_{pqkl}l_k n_l]\,[\int_F b(\mathbf{y})\,dS]S(t)$$
$$= [C_{pqkl}l_k n_l]\,\Delta V\,S(t) = m_{pq}\,S(t), \qquad (1)$$

where C_{pqkl} is the tensor of elastic constants and ΔV is the crack volume. As seen in eq. 1, the moment tensor has the dimension of moment [Nm], because of [elastic constants: N/m^2] times [crack volume: m^3]. Corresponding to AE wave motion, elastic displacement $\mathbf{u}(\mathbf{x},t)$ is represented as,

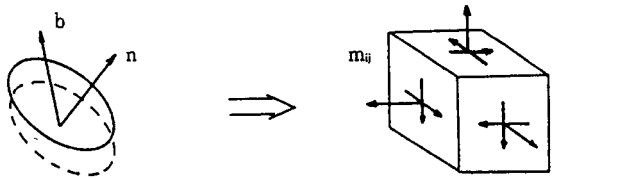

Figure 1. Crack motion and moment tensor

$$u_i(\mathbf{x},t) = G_{ip,q}(\mathbf{x},\mathbf{y},t)\, m_{pq} * S(t). \quad (2)$$

Here $G_{ip,q}(\mathbf{x},\mathbf{y},t)$ is the spatial derivatives of Green's functions and the asterisk * denotes the convolution operation. In the SiGMA code, eq. 2 is simplified, taking into account only the amplitude of the first motion $A(\mathbf{x})$,

$$A(\mathbf{x}) = Cs / R \bullet Ref(\mathbf{t},\mathbf{r})\, r_p\, m_{pq}\, r_q, \quad (3)$$

where Cs is the calibration coefficient. R is the distance and $\mathbf{r}$ or r_p is its direction vector. $Ref(\mathbf{t},\mathbf{r})$ is the reflection coefficient associated with incident direction $\mathbf{r}$ and orientation of sensor sensitivity $\mathbf{t}$. A multi-channel observation of the first motions at more than six sensor locations is necessary and sufficient to solve eq. 3.

(2) Eigenvalue Analysis

In order to elucidate principal motions on the crack surface, three eigenvalues of the moment tensor are introduced. Assuming that the tensor components consist of both tensile contribution and shear contribution, the eigenvalues normalized are uniquely decomposed into three ratios X, Y, and Z (Ohtsu, 1991)

$$\begin{aligned} &1.0 = X + Y + Z, \\ &\text{the intermediate eigenvalue/the maximum:E2} \\ &\quad = 0 - Y/2 + Z, \\ &\text{the minimum eigenvalue/the maximum:E3} \\ &\quad = -X - Y/2 + Z, \end{aligned} \quad (4)$$

where X, Y, and Z denote the shear ratio, the deviatoric tensile ratio, and the isotropic tensile ratio, respectively. The decomposition is illustrated in Fig. 2. In the SiGMA procedure, AE sources for which the shear ratios X are smaller than 40% are classified as tensile cracks and those of the shear ratio X greater than 60% are referred to as shear cracks. In the case between 40% and 60%, AE sources are classified as mixed-mode. In order to take a point explosion into consideration, another decomposition was proposed by Shah and Labuz (1995). Their new component, however, is essentially represented by the ratio Z. In addition, it is not reasonable to add another term to the moment tensor, because the tensor is theoretically derived from the dislocation model.

After the eigenvalue analysis, unit eigenvectors **e1**, **e2** and **e3** are obtained. These correspond theoretically to three vectors $\mathbf{l} + \mathbf{n}$, $\mathbf{l} \times \mathbf{n}$ and $\mathbf{l} - \mathbf{n}$. Thus, crack vector $\mathbf{l}$ and crack normal $\mathbf{n}$ can be recovered from the following relations,

$$\begin{aligned} \mathbf{l} &= [(2 + 2l_k n_k)\mathbf{e1} + (2 - 2l_k n_k)\mathbf{e3}]/2, \\ \mathbf{n} &= [(2 + 2l_k n_k)\mathbf{e1} - (2 - 2l_k n_k)\mathbf{e3}]/2. \end{aligned} \quad (5)$$

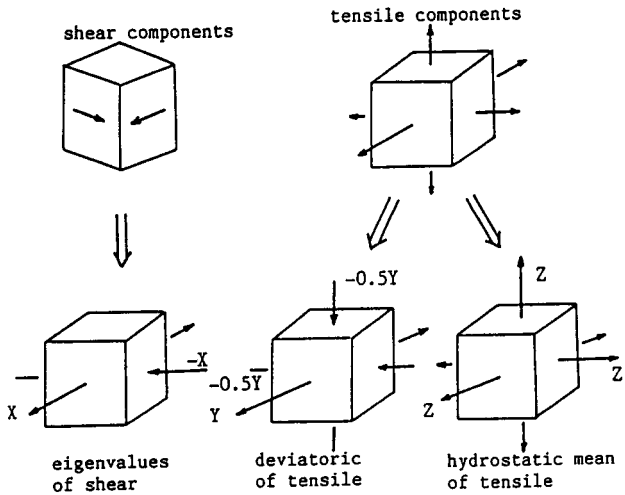

Figure 2. Unified decomposition of the eigenvalues.

Here the scalar product $l_k n_k$ is equal to (1 + E3 - 2E2)/(1 - E3). It is noted that the vectors **l** and **n** are interchangeable.

(3) Damage Parameter

From eq. 1, moment tensor m_{pq} is obtained in an isotropic material, as follows:

$$m_{pq} = [C_{pqkl} l_k n_l]\Delta V = [\lambda l_k n_k d_{pq} + \mu l_p n_q + \mu l_q n_p]\Delta V, \tag{6}$$

where λ and μ are Lame constants. In damage mechanics, a product of the crack motion vector and the crack normal is referred to as a damage tensor. Taking into account one crack, it is represented as,

$$\begin{aligned} d_{kl} &= 1/V^* \int_F ([b(\mathbf{y})l_k]\, n_l + [b(\mathbf{y})l_l]\, n_k)\, dS / 2 \\ &= (l_k n_l + l_l n_k)\, \Delta V / (2V^*). \end{aligned} \tag{7}$$

where V* is the representative volume. Thus, scalar damage parameter D for one crack is obtained as,

$$D = n_k\, d_{kl}\, n_l = l_k n_k\, \Delta V / V^*. \tag{8}$$

From eq. 6, the trace component of the moment tensor is derived as,

$$m_{kk} = (3\lambda + 2\mu)\, l_k n_k \Delta V. \tag{9}$$

Comparing eq. 9 with eq. 8, it is found that damage parameter D is equivalent to the trace component of the moment tensor. This implies that damage evolution could be estimated from the accumulation of the trace components of the moment tensor, m_{kk}.

(4) Crack Volume

Based on eq. 9, the crack volume is obtained from,

$$\Delta V = m_{kk} / [(3\lambda+2\mu) l_k n_k]. \quad (10)$$

As discussed in eq. 5, the scalar product $l_k n_k$ can be determined from the eigenvalues. From eq. 10, it is realized that the crack volume is also obtained from the trace component of the moment tensor. To determine the crack volume, however, the moment tensor should be determined as calibrated values. This implies that AE sensors must be calibrated prior to the experiment. It is noted that sensor calibration is not necessary for the standard SiGMA procedure, because only relative values are applied to the eigenvalue analysis.

(5) Stress Intensity Factors

In Fig.3, the direction θ of crack extension from a pre-existing crack is determined from the direction of the maximum circumferential stress in LEFM by Erdogan and Sih (1963) as,

$$K_I \sin\theta + K_{II}(3\cos\theta - 1) = 0. \quad (11)$$

Here, K_I and K_{II} are the stress intensity factors of the mode I and the mode II, respectively. Initiation of crack extension is governed by,

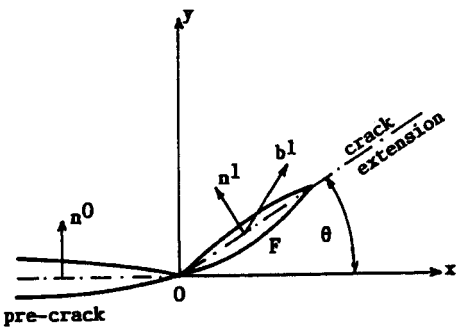

Figure 3. Crack extenstion from the pre-exisiting crack.